Testing the Sensitivity of the Extratropical Response to the Location, Amplitude, and Propagation Speed of Tropical Convection

MICHAEL GOSS AND STEVEN B. FELDSTEIN

Department of Meteorology, The Pennsylvania State University, University Park, Pennsylvania

(Manuscript received 25 April 2017, in final form 28 November 2017)

ABSTRACT

The dynamical core of a dry global model is used to investigate the role of central Pacific versus warm pool tropical convection on the extratropical response over the North Pacific and North America. A series of model runs is performed in which the amplitude of the warm pool (WP) and central Pacific (CP) heating anomalies associated with the MJO and El Niño–Southern Oscillation (ENSO) is systematically varied. In addition, model calculations based on each of the eight MJO phases are performed, first using stationary heating, and then with heating corresponding to a 48-day MJO cycle and to a 32-day MJO cycle.

In all model runs, the extratropical response to tropical convection occurs within 7–10 days of the convective heating. The response is very sensitive to the relative amplitude of the heating anomalies. For example, when heating anomalies in the WP and CP have similar amplitude but opposite sign, the amplitude of the extratropical response is much weaker than is typical for the MJO and ENSO. For the MJO, when the WP heating anomaly is much stronger than the CP heating anomaly (vice versa for ENSO), the extratropical response is amplified. For the MJO heating, it is found that the extratropical responses to phases 4 and 8 are most distinct. A likely factor contributing to this distinctiveness involves the relative amplitude of the two heating anomalies. The stationary and moving (48- and 32-day) heating responses are very similar, revealing a lack of sensitivity to the MJO phase speed.

1. Introduction

Large regions of anomalous equatorial convection associated with two key atmospheric phenomena are known to significantly impact extratropical circulation patterns. The first is the El Niño–Southern Oscillation (ENSO; e.g., Rasmusson and Carpenter 1982; Rasmusson and Wallace 1983), with a seasonal time scale. The second is the Madden–Julian oscillation (MJO; Madden and Julian 1971, 1972), which is associated with equatorial convective anomalies that propagate eastward, and has a period of 30–60 days. The MJO is typically separated into eight phases, which correspond to the longitude of the convective anomalies (Wheeler and Hendon 2004, hereafter WH). ENSO is categorized into El Niño and La Niña periods, when the SST anomalies in the equatorial central and eastern Pacific are warm and cool, respectively, and those periods outside of El Niño and La Niña are considered ENSO neutral. Modeling and observational studies, such as Hoskins and Karoly (1981) and Yoo et al. (2012a, b), show that the extratropical response to tropical heating occurs within 7–10 days. Because tropical forcing occurs on subseasonal to seasonal (S2S) time scales, an understanding of these equatorial phenomena and their impacts on the extratropics can aid in extratropical predictability on the S2S time scales (Zhang et al. 2013; Johnson et al. 2014).

Previous modeling studies have shown a large sensitivity of the extratropical response to the longitudinal location of convective heating over the equatorial Pacific basin. For example, studies such as Ting and Sardeshmukh (1993) using idealized heating in a dry general circulation model (GCM), and Barsugli and Sardeshmukh (2002) using SST forcing in a simple GCM with parameterized convection, both show that the modeled spatial pattern response over the extratropical North Pacific and North America is highly sensitive to the longitudinal location of the heating source over the equatorial Pacific. Additionally, a recent modeling and observational study by Goss and Feldstein (2017) found that differences in the extratropical response to similar convective patterns are explained by the relative strength and amplitude of warm pool (WP) and central Pacific (CP) tropical convection. In that study, the pattern correlation

Corresponding author: Michael Goss, goss@stanford.edu

DOI: 10.1175/JAS-D-17-0132.1

© 2018 American Meteorological Society. For information regarding reuse of this content and general copyright information, consult the AMS Copyright Policy (www.ametsoc.org/PUBSReuseLicenses).

Brought to you by NOAA Central Library | Unauthenticated | Downloaded 02/01/21 04:56 PM UTC

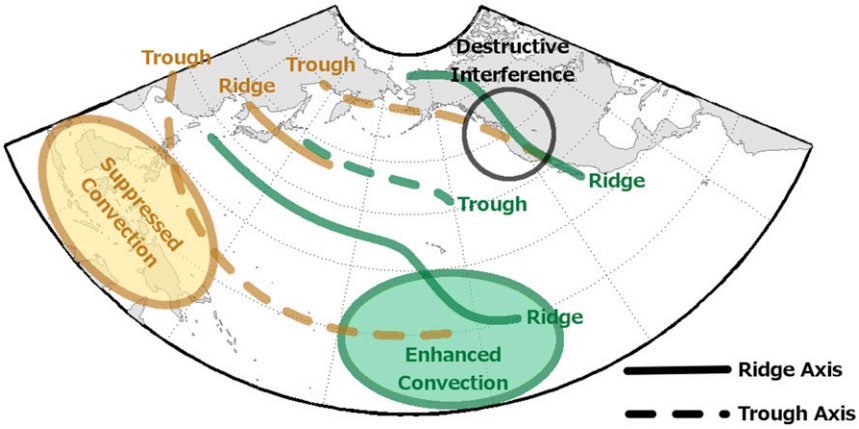

FIG. 1. Schematic diagram of the model 0.3σ height response to isolated suppressed WP convection (brown) and to isolated enhanced CP convection (green). Trough axes are shown as dashed lines, and ridge axes are shown as solid lines. A region where the response to WP and CP convection is of opposite sign is highlighted with a black circle.

between the tropical precipitation composites for El Niño and MJO phase 1 was found to be 0.58, which was statistically significant at the 99.9th percentile. The pattern correlation between the tropical precipitation composites for La Niña and MJO phase 5 was lower at 0.39 but was still significant at the 96.1th percentile. However, even though the precipitation composites were similar, the geopotential height response is seen to be of opposite sign over the northeastern North Pacific and northwestern North America. With both model and observational data, it was found that the extratropical response to a single isolated enhanced convection anomaly in either the WP or CP resembles the positive phase of the Pacific–North America (PNA) teleconnection pattern, though with a longitudinally shifted response likely associated with the longitudinal shift of the isolated forcing. Analogously, a suppressed convection anomaly over the WP or CP gives rise to the negative phase of the PNA, but with a similar longitudinal shift. Moreover, with the same model and observational data, it was shown that the extratropical response to more than one convection anomaly could largely be explained as a linear summation of the response to separate single convection anomalies from different subdomains. In the response to convection associated with either ENSO or the MJO, it was seen that the weaker of the two convective signals, which is almost always of opposite sign, drives some cancellation in the extratropical response. This cancellation occurs because there are regions where the geopotential height response to an isolated negative WP convection anomaly is opposite to that for an isolated positive CP convection anomaly and vice versa when the sign of the convection anomalies is reversed. This is illustrated by overlapping ridge and trough axes in the schematic diagram (see Fig. 1) for the case of suppressed WP convection and enhanced CP convection. Based on these results, it is conceivable that there sometimes exists a convective pattern that features near-equal-amplitude CP and WP convective anomalies of opposite sign, which would force a very weak, near-zero-amplitude response over portions of the North Pacific and northwestern North America, owing to cancellation of the opposite-signed responses over that region. Furthermore, it is also likely that there are times when either the WP or the CP convection dominates much more than would be expected from the MJO or ENSO composites. During these times, an exceptionally large-amplitude PNA could be expected. Such patterns, when the WP or CP convection dominates more than usual, may arise in observations during particular combinations of ENSO and MJO phase and amplitude. Therefore, a study of the continuum of possible WP and CP combinations may aid in better understanding the extratropical response to each unique individual ENSO or MJO on a case-by-case basis.

In the modeling part of the study by Goss and Feldstein (2017), the heating was held at a constant amplitude, and at a fixed geographical location, for 10 days. However, in observations, convective anomalies associated with the MJO gradually propagate eastward in time, such that a full MJO cycle tends to complete in about 30–60 days (Madden and Julian 1971, 1972; WH; and others). The important question of how a more realistically propagating MJO-like convective heating, with various phase speeds, might impact the extratropical response to the tropical

Brought to you by NOAA Central Library | Unauthenticated | Downloaded 02/01/21 04:56 PM UTC

convection was not addressed. (Most previous idealized modeling studies of the extratropical response to the MJO also kept the heating fixed; e.g., Seo and Son 2012; Yoo et al. 2012b.) Moreover, Goss and Feldstein (2017) focused on MJO phases 1 and 5, since those phases have convective patterns with a similar spatial structure as those associated with El Niño and La Niña, respectively. The other six MJO phases were not modeled. A more complete understanding of the sensitivity of the extratropical responses to stationary versus moving MJO heating, as well as the response to all eight MJO phases, might also further help to enhance extratropical predictability when the MJO is active.

With the above in mind, the purpose of this study is to address the following four key questions in a simple dynamical model: 1) How does the systematic variation of the strength of WP and CP convection anomalies associated with MJO phases 1 and 5, and El Niño and La Niña, affect the extratropical response? 2) What is the modeled extratropical response to stationary heating using realistic precipitation composites for all eight MJO phases? 3) What is the sensitivity of the modeled extratropical response to stationary versus realistic eastward-propagating MJO-like convection for each of the eight phases? 4) What is the sensitivity of the modeled extratropical response to the propagation speed of MJO-like convection for each of the eight phases?

Section 2 describes the methods used in the study. Section 3 examines the impact of varying WP and CP convection for ENSO-like and MJO-like composites. Section 4 is a study of the sensitivity of the model results to a stationary versus a moving heating source. Finally, section 5 contains a summary of the results and the conclusions of the study.

2. Methods

For the study, we use the dry dynamical core of the National Oceanic and Atmospheric Administration/Geophysical Fluid Dynamics Laboratory (NOAA/GFDL) spectral climate model at triangular 42 horizontal resolution, with 19 vertical sigma (σ) levels. At sigma levels greater than 0.7, Rayleigh friction is applied, with a damping time scale that increases vertically from 1 day at the surface, as in Held and Suarez (1994). No vertical diffusion term is included. However, fourth-order horizontal diffusion is included with a time scale of 0.1 days at the model's smallest resolvable scale. We use radiative relaxation to force the model. Specifically, Newtonian cooling acts upon the perturbation temperature. Here, a perturbation refers to a deviation from the model's initial state, which is defined as the observed December–February (DJF) climatology for the years 1979–2012. Data for the mean climatological state is obtained from the European Centre for Medium-Range Weather Forecasts interim reanalysis (ERA-Interim) dataset (Dee et al. 2011). The climatology defined above is not a balanced state in the model. Balance is achieved by adding a forcing term to the model equations. This forcing term is obtained by integrating the model equations forward in time by one time step, using the climatological state as the initial flow.

Forcing due to tropical convection is approximated in the model by converting precipitation composites into heating composites, as in Goss and Feldstein (2015, 2017) and Yoo et al. (2012b). Composites of precipitation are derived from a daily interpolation of NOAA/Climate Prediction Center (CPC) Merged Analysis of Precipitation (CMAP) data (Xie and Arkin 1997). The precipitation rates from these composites are converted to heating rates by multiplying the precipitation rate by the latent heat of vaporization of water and the density of water, then dividing by the heat capacity of water at constant pressure, the density of air, and the vertical scale. The heating field at latitudes outside of the 30°S–30°N band is set to 0, and a cosine-squared function with zeros at the bounds is used to define weighting of the heating field between 30°S and 30°N. This defines the horizontal structure of the heating field. The vertical structure is prescribed as in Yoo et al. (2012b), with a maximum heating anomaly located at the $\sigma = 0.5$ level. They found that altering the vertical profile had an impact on the amplitude of the response but little impact on the spatial pattern of the response. For each model run, heating is ramped up during the first model day and ramped down during the last model day.

Various precipitation composites based on the phases of ENSO and the MJO are calculated for use in the model experiments. For El Niño days, we use the CPC definition for ENSO events. If the oceanic Niño index (ONI), which is based on the Niño-3.4 region, is greater than 0.5 for at least five consecutive 3-monthly periods, all consecutive central months are considered El Niño months, and all days within the DJF central months are treated as El Niño days. La Niña days are found using an analogous method, but for those cases where ONI is less than −0.5 for at least five consecutive 3-monthly periods. For the MJO composites, we use the definition of MJO amplitude and phase from WH—specifically, the real-time multivariate MJO (RMM) 1 and RMM2 indices, the first two principal component time series of the combined empirical orthogonal functions of the

Brought to you by NOAA Central Library | Unauthenticated | Downloaded 02/01/21 04:56 PM UTC

tropical 200- and 850-hPa zonal wind and outgoing longwave radiation. RMM1 and RMM2 are used to define the two axes of a Cartesian diagram, split by angles into eight "phases." The length of a vector from the origin to (RMM1, RMM2) for a given day is defined as the MJO amplitude for that day. For the stationary heating composites, for each of the eight MJO phases, we include all DJF days in a given phase with an MJO amplitude greater than 1.0. A discussion of the methods used to determine composites and model forcing for the moving convection cases can be found below.

The model is run 56 times using a different heating field for each case. For the first 32 model runs, the heating is stationary. The precipitation composites used for the first set of 16 model runs are seen in Fig. 2.[1] Each precipitation composite is limited to the domain from 15°S to 15°N and from 90°E to 150°W. Figure 1f corresponds to a composite of precipitation for El Niño days, and Fig. 2k corresponds to a composite of precipitation for MJO phase 1 days. Figures 2g–j correspond to a linear transition at each grid point from Figs. 2f–k, in which the negative anomaly over the WP is gradually strengthened, and the positive anomaly over the CP is gradually weakened. For Figs. 2a–e, the El Niño composite is again used, but the WP contribution from the domain 90°–150°E is multiplied by factors increasing from 0.0 through 0.8, in increments of 0.2, with the CP positive heating anomaly remaining constant. In Figs. 2l–p, the MJO phase 1 composite is used, with the CP contribution from the domain 175°E–150°W being multiplied by factors decreasing from 0.8 to 0.0, in increments of 0.2, and the WP anomaly being kept constant. Figure 3, corresponding to the next set of 16 model runs, is constructed identically, with El Niño being replaced by the La Niña and MJO phase 1 by MJO phase 5.

The next eight model calculations are also run with stationary heating and correspond to the eight phases of the MJO (see Fig. 4). For the final 16 model calculations, a moving heating source is used. Two sets of model calculations are performed for each MJO phase: the first corresponding to a 48-day MJO cycle and the second to a 32-day MJO cycle. To find realistic precipitation composites for a 48-day MJO cycle, the RMM1–RMM2 Cartesian diagram is first divided into 48 equal-angle bins, with bounds ranging from 0 to 2π every $\pi/24$ (this is analogous to the splitting of the MJO cycle into eight phases in WH). For the 32-day cycle, angle-bin bounds are separated by $\pi/16$. For each DJF day, using the RMM1 and RMM2 indices, an angle is calculated from the RMM1 axis, and the corresponding angle bin is found for each day. For the 48-day MJO cycle, the first six angle bins above the RMM1 axis, labeled angle bins 1–6, correspond to MJO phase 5 of WH, the next six labeled angle bins correspond to MJO phase 6 of WH, and so on around the Cartesian diagram. This leads to the calculation of 48 composites for the 48-day MJO cycle, one for each bin. The 48-day MJO cycle is temporally smoothed at each grid point by removing variability with a time scale shorter than 16 days using a Fourier filter. Analogously, for the 32-day cycle, the first four angle bins above the RMM1 axis, labeled 1–4, correspond to MJO phase 5, the next four to MJO phase 6, and so on, for 32 total composites. Variability shorter than 10⅔ days is removed in this case.

For each MJO phase of the 48-day MJO cycle, model days 1–15 correspond with angle bins ranging from the last two angle bins of the previous phase, the six angle bins of the current phase, the six angle bins of the following phase, and the first angle bin two phases later. For the 32-day MJO cycle, a wider range of MJO phases is used. Days 1–15 include the last three angle bins of the previous phase, the four angle bins of the current phase, the four angle bins of the next two phases, and the first angle bin three phases later. For example, in the 48-day case, for MJO phase 5, angle bins 47, 48, and 1–13 are used to force model days 1–15, respectively. These correspond to the last two angle bins of MJO phase 4, all six angle bins of MJO phases 5 and 6, and the first angle bin of MJO phase 7. By analogy, in the 32-day case, angle bins 30–32 and 1–13 are used to force model days 1–15, respectively. These angle bins correspond to the last three angle bins of MJO phase 4; all four angle bins of MJO phases 5–7; and the first angle bin of MJO phase 8. The angle bins are chosen in order that days 5 and 6 of the model heating correspond to the middle of the particular MJO phase. The heating field for each time step is linearly interpolated from the two angle bins corresponding with the two nearest model days; that is, for MJO phase 5 in the 48-day cycle case, for the model time step halfway between model days 3 and 4, the total heating receives a 50% contribution from angle bins 1 and 2.

3. Warm pool and central Pacific heating

Figure 5 shows, for model days 12–15, the 0.3σ extratropical height anomaly response to the heating fields defined by the precipitation composites in Fig. 2, with Fig. 5f corresponding to the response to El Niño–like convection, and Fig. 5k corresponding to the response to MJO phase 1–like convection. As indicated in the introduction, these

[1] Note that cool colors correspond to positive anomalous precipitation and warm colors to negative anomalous precipitation.

Brought to you by NOAA Central Library | Unauthenticated | Downloaded 02/01/21 04:56 PM UTC

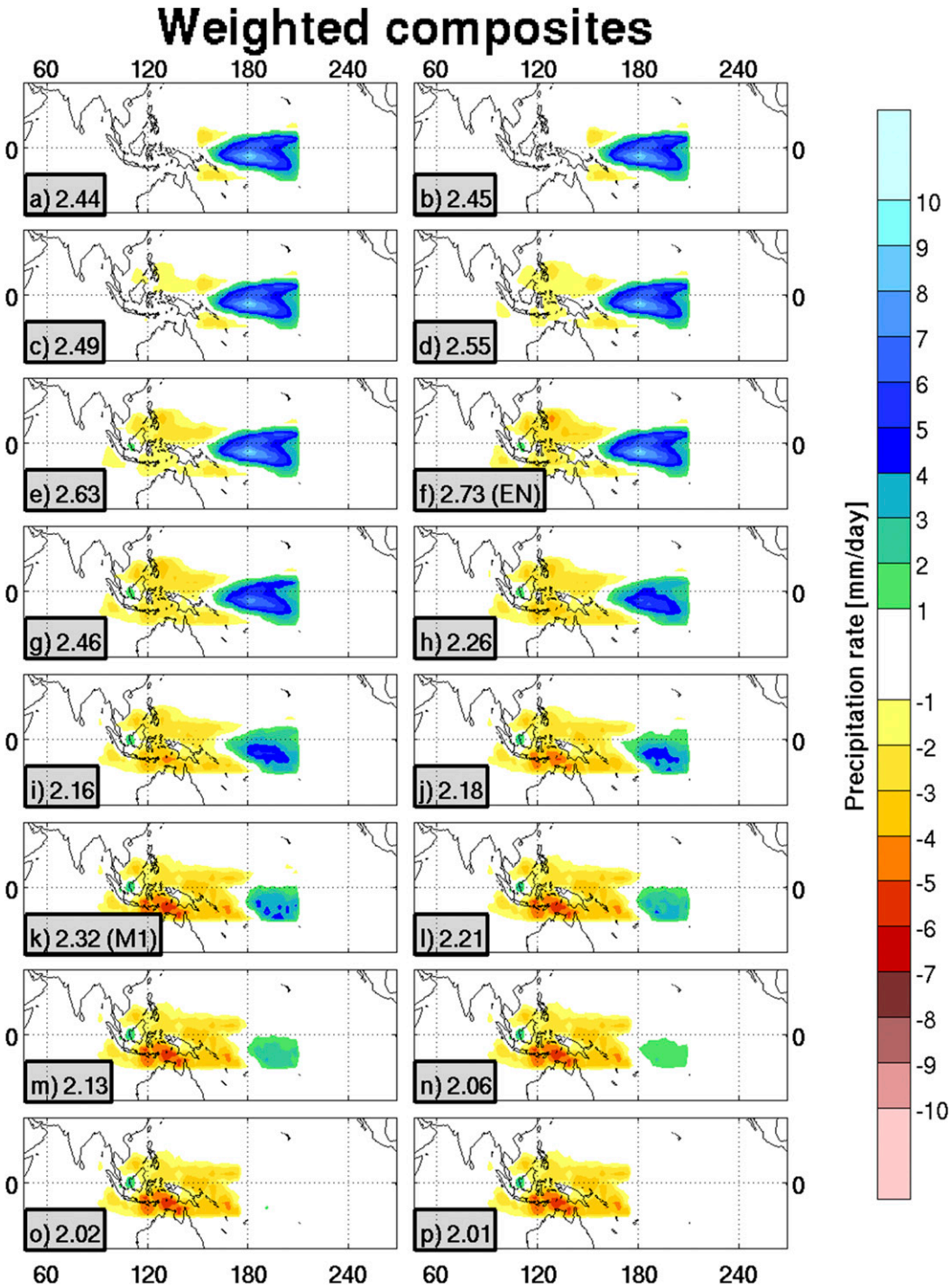

FIG. 2. El Niño and MJO phase 1 precipitation anomaly composites. (a)–(f) El Niño composites, with a warm pool component (see text) increasing from 0% to 100% with an interval of 20%. (g)–(j) A blend of El Niño and MJO phase 1 composites, with the El Niño component decreasing from 80% weighting to 20% weighting with an interval of 20%. (k)–(p) MJO phase 1 composites, with a central Pacific component (see text) decreasing from 100% to 0% with an interval of 20%. Values in the gray boxes are the root-mean-squared anomalies from 15°S to 15°N and from 90°E to 150°W.

Brought to you by NOAA Central Library | Unauthenticated | Downloaded 02/01/21 04:56 PM UTC

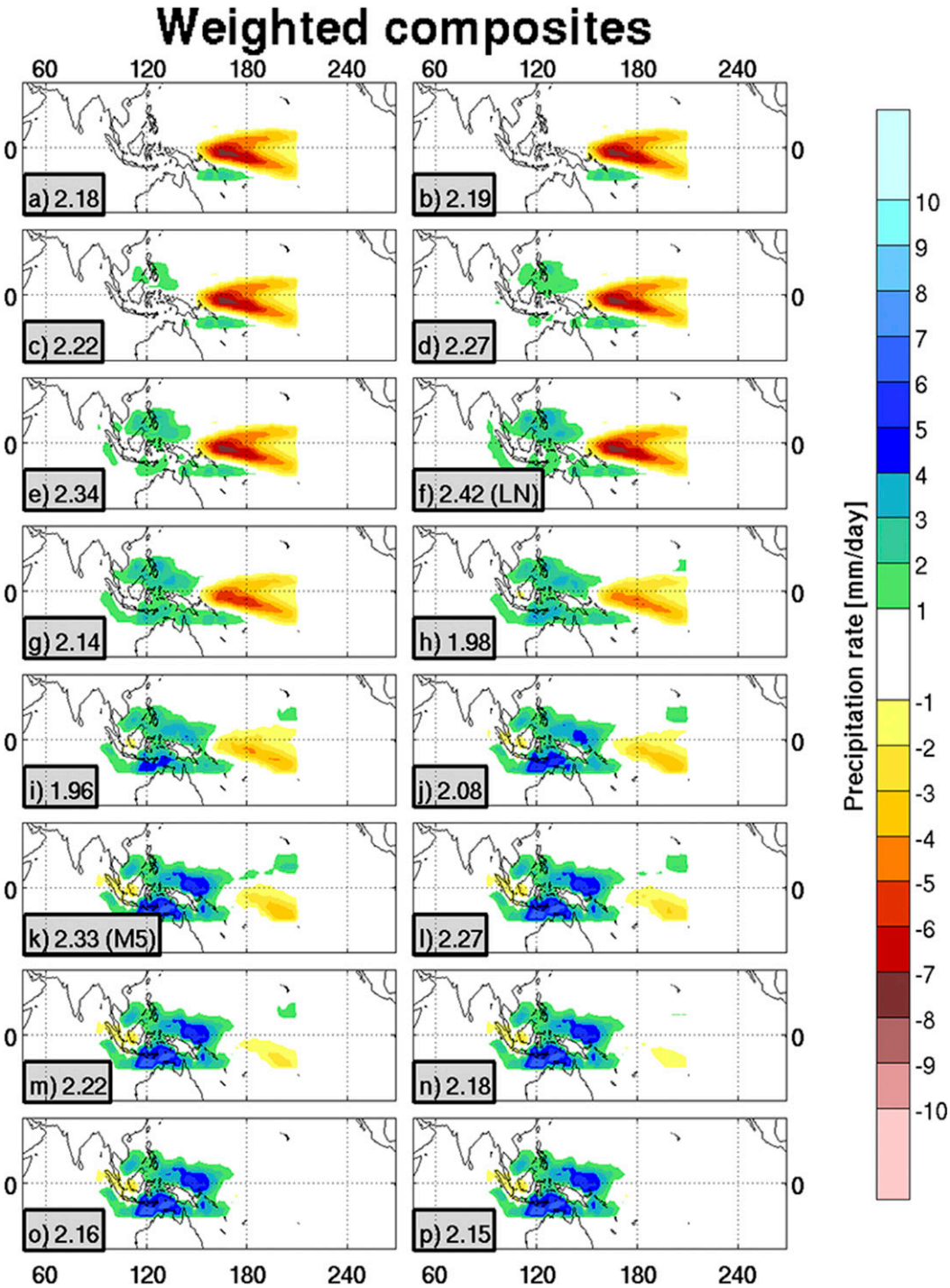

FIG. 3. As in Fig. 2, but for the La Niña and MJO phase 5 case.

two base cases are chosen because the precipitation composites for El Niño and MJO phase 1 have a similar spatial structure, with different amplitudes and extratropical responses over the North Pacific and North America (Goss and Feldstein 2017). We see that the responses over the northeastern Pacific and North America to convective fields that are a blend of El Niño and MJO phase 1 convection (Figs. 5f–k) gradually transition from an increasingly weaker El Niño–like response (Figs. 5f–i), to a response that has characteristics of both El Niño and MJO

Brought to you by NOAA Central Library | Unauthenticated | Downloaded 02/01/21 04:56 PM UTC

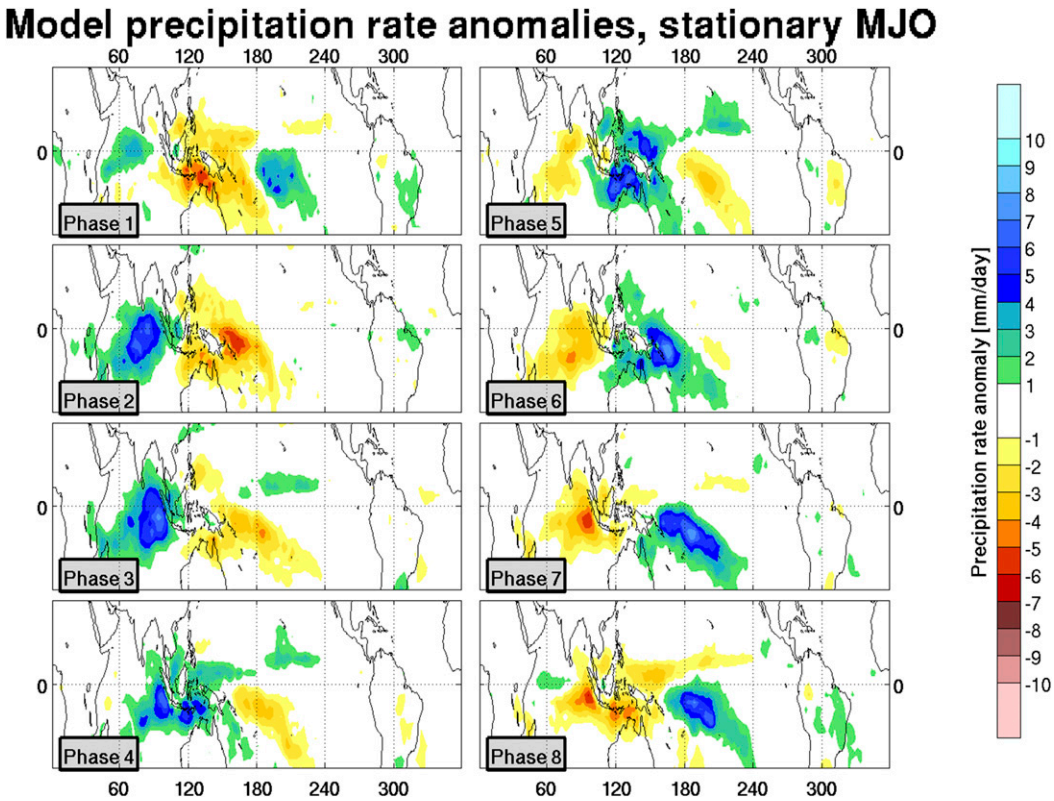

FIG. 4. Precipitation anomaly composites for MJO phases 1–8.

phase 1 (Fig. 5j), to the MJO phase 1 response in Fig. 5k. This corresponds to a transition from a spatial pattern that resembles the positive PNA to a pattern that resembles the negative PNA, but with anomalies located over the northwestern Pacific. Specifically, the positive height anomaly over northwestern North America in Fig. 4f gradually decreases until it is gone entirely by Fig. 5k. The negative height anomaly over the central North Pacific in Fig. 5f gradually weakens and expands both eastward over the northeastern Pacific until it is extends from Siberia to the western coast of North America. Also, the positive height anomaly in the Northern Hemisphere tropics transitions into a negative anomaly. For Figs. 5a–f, corresponding to the gradual introduction of the negative WP convective anomaly of El Niño, we see that the spatial structure of the response remains largely unchanged, though the amplitude of the response over the subtropics gradually weakens. Finally, for Figs. 5k–p, corresponding to the gradual removal of the CP convective anomaly of MJO phase 1, the negative height anomaly over the northeastern Pacific merges with the negative height anomaly over northern South America, while separating from the negative height anomaly over the northeastern Pacific. The overarching conceptual picture is that the response over the North Pacific and North America depends strongly on the relative amplitude of the convective signals over the WP and the CP, that the El Niño response is dominated by the CP signal and the MJO phase 1 response is dominated by the WP signal, and that the transition features very weak anomaly responses over the far northeastern Pacific and the western coast of North America, that is, much of the PNA region.

The numerical value in each panel of Fig. 5 is the square root of the spatial mean of the squared height anomalies (or the average absolute anomalies) for the domain with bounds 20°–75°N and 135°–105°W. This region shows opposite-signed height anomalies in the response to CP and WP anomalies (cf. Figures 5a and 5p) and, thus, is the main region where we would expect to see cancellation between the response to CP and WP precipitation anomalies. Analogous numerical values are included in Fig. 2, which show the average absolute precipitation anomalies for the domain with bounds 15°S–15°N and 90°–150°W. In this way, we can compare a measure of the strength of the overall precipitation signal with the strength of the height response over a particular region of the extratropics. We see that, although the weakest precipitation signal is found in Fig. 2p (2.01 mm day^{-1}), corresponding to MJO phase 1 with CP convection completely removed, the weakest

Brought to you by NOAA Central Library | Unauthenticated | Downloaded 02/01/21 04:56 PM UTC

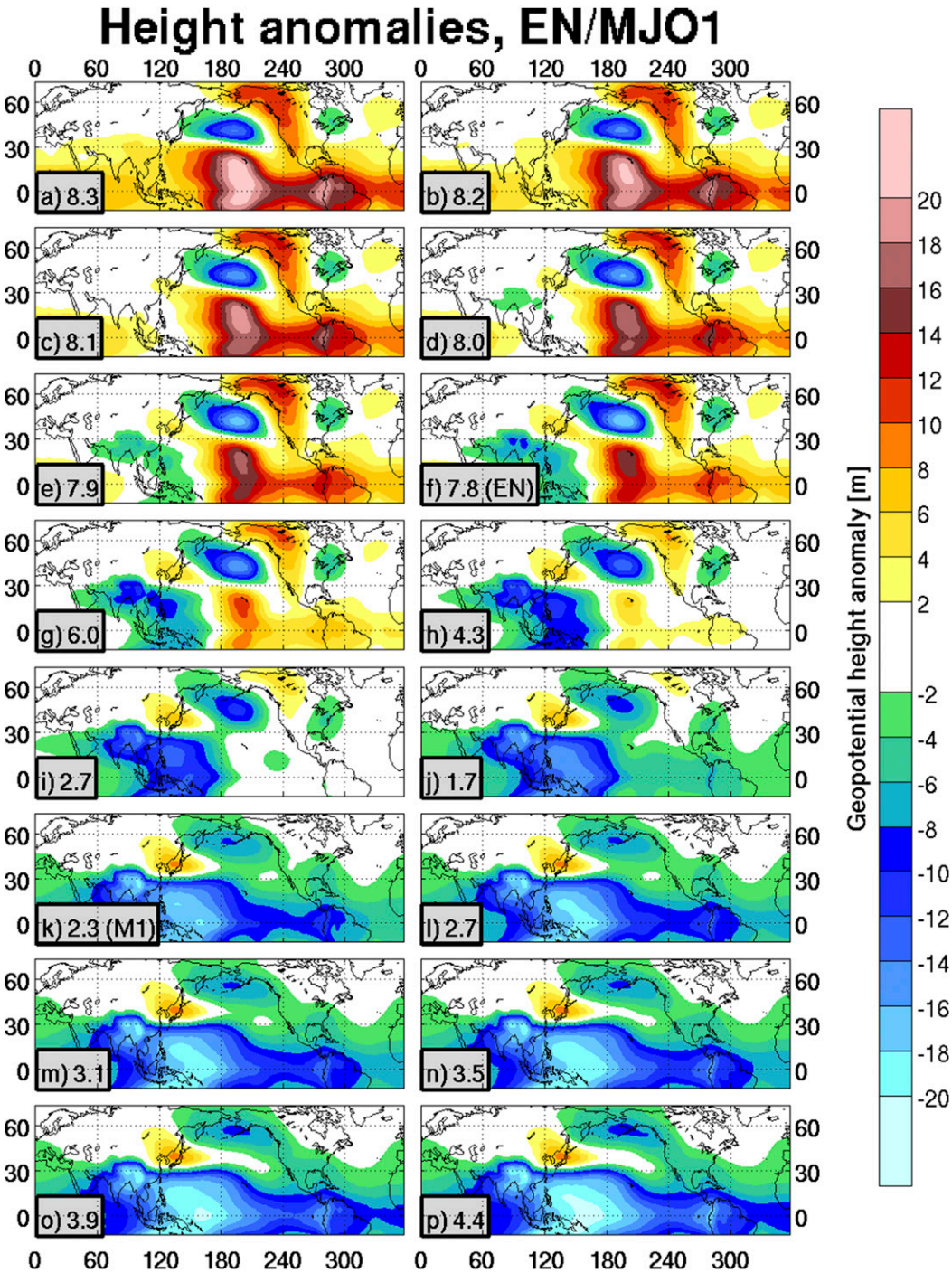

FIG. 5. For model days 7–10, the 0.3σ height anomaly response to heating based on the precipitation composites in the corresponding panels in Fig. 1. Values in the gray boxes are the root-mean-squared height anomalies from 20° to 75°N and from 135° to 105°W.

response is in Fig. 5j (1.7 m), in the transition between the response to El Niño and MJO phase 1 convection. This result is consistent with the idea that there is some cancellation between the positive height anomaly response seen along the western coast of North America with strong CP convection (Fig. 5a) and the negative height anomaly response over the same region seen with anomalously weak WP convection (Fig. 5p). Therefore,

Brought to you by NOAA Central Library | Unauthenticated | Downloaded 02/01/21 04:56 PM UTC

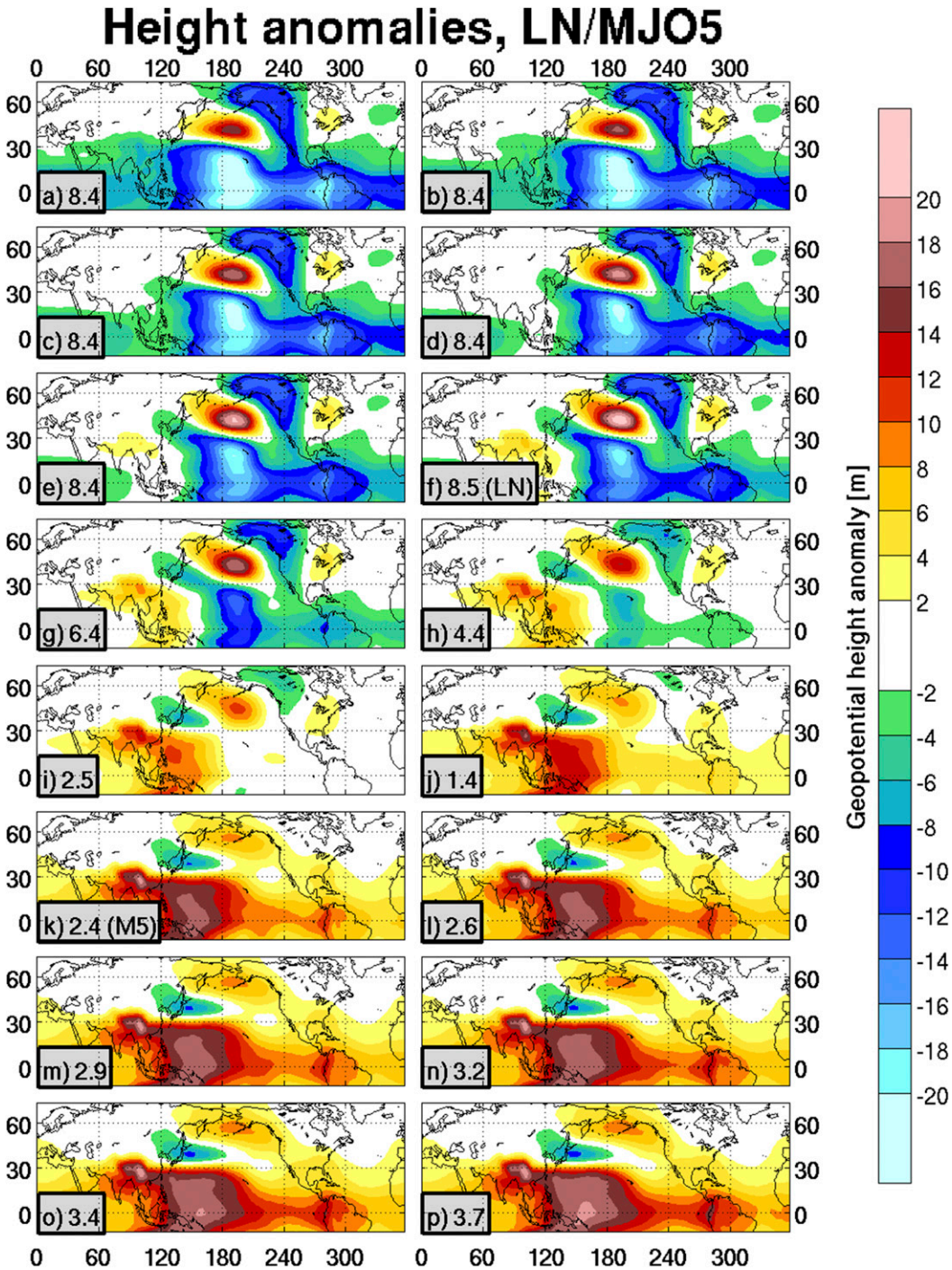

FIG. 6. As in Fig. 5, but for heating based on the precipitation composites in the corresponding panels in Fig. 3.

because of this cancellation, even though the strength of the overall precipitation signal is not appreciably weaker in Figs. 2j and 2k than in many of the other cases, the strength of the height response over the northeastern Pacific and the western coast of North America is much weaker. These results are also consistent for the MJO phase 1 model runs (Figs. 5k–p), where the strongest extratropical response (Fig. 5p) coincides with the weakest CP and overall precipitation. The El Niño model runs (Figs. 5a–f) also show weak cancellation over the height domain chosen. The extratropical response shows the largest amplitude response (Fig. 5a)

Brought to you by NOAA Central Library | Unauthenticated | Downloaded 02/01/21 04:56 PM UTC

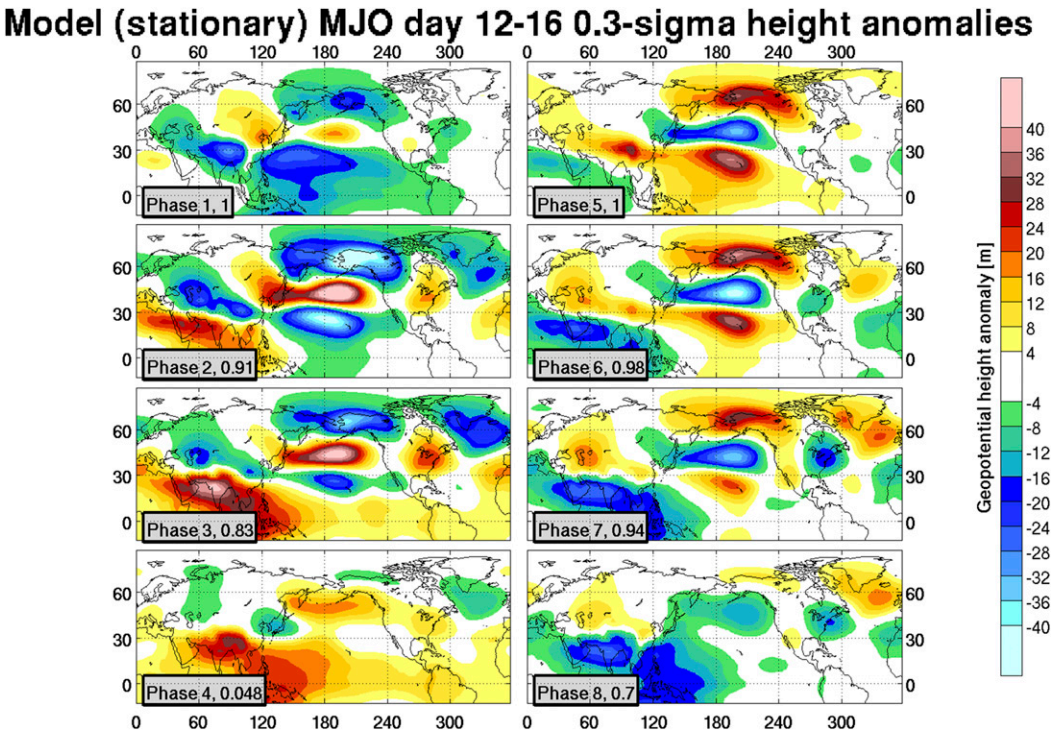

FIG. 7. For model days 12–16, the 0.3σ height anomaly response to stationary heating for each MJO phase. Values in the gray boxes are the pattern correlations from 30° to 75°N and from 180° to 90°W between the MJO phase 1 response to stationary convection and the patterns in the panels that correspond to phases 1–4 and between the MJO phase 5 response to stationary convection and the patterns in the panels that correspond to phases 5–8.

when the WP precipitation is completely removed (Fig. 2a). There is a small region of opposite-signed anomalies seen in Figs. 5a and 5p over the North Pacific just west of the international date line, but they are not well aligned and cancellation only occurs over a much smaller region. Additionally, there is a region near the Aleutian Islands where Figs. 5a and 5p both show negative anomalies, and therefore, instead of cancellation, the negative anomalies are enhanced when both CP and WP precipitation anomalies are present. These regions are not the focus of this manuscript, however. Taken as a whole, these results highlight the tendency for there to be cancellation between the extratropical response over the northeastern Pacific and the western coast of North America to tropical precipitation anomalies in the WP and CP when these precipitation anomalies are of opposite sign.

For the La Niña–MJO phase 5 precipitation composites (Fig. 6), the results are mostly analogous to those for El Niño–MJO phase 1. The responses in Fig. 6 largely have the same spatial structure with the opposite sign as those in Fig. 5. There is a strong negative height anomaly over northwestern North America and the far northeastern North Pacific, associated with the CP convective anomaly that is most predominant in the La Niña convective fields (Figs. 6a–f). For the transition model runs (Figs. 6f–k), this negative height anomaly vanishes, there is an eastward and westward expansion of the North Pacific positive anomaly, and a change from a negative to a positive height anomaly over the Northern Hemisphere subtropics. As with El Niño–MJO phase 1, the weakest response over the northeastern Pacific and the western coast of North America is seen in Fig. 6j (1.4 m), associated with a mean squared precipitation composite value in Fig. 3j (2.08 mm day^{-1}). This is in spite of the fact that the strength of the total precipitation composite is weakest in Figs. 3h and 3i (1.98 and 1.96 mm day^{-1}, respectively), while the response in Figs. 6h and 6i (4.4 and 2.5 m, respectively), is significantly stronger. This, again, suggests that cancellation between the response to strong WP convection and strong CP convection can lead to a very weak response over the northeastern Pacific and the western coast of North America. Like with Fig. 5, we see that the extratropical response is also most intense for MJO phase 5 case when WP convection is present with no CP convection. The La Niña results are inconsistent with cancellation, with the average absolute height anomalies

Brought to you by NOAA Central Library | Unauthenticated | Downloaded 02/01/21 04:56 PM UTC

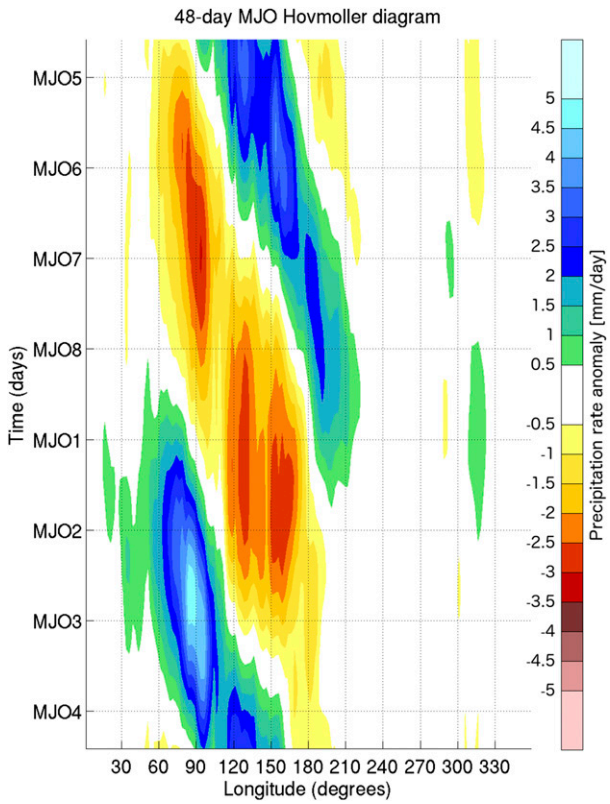

FIG. 8. Hovmöller diagram of the precipitation-rate anomaly for the 48-day MJO cycle (see text). Precipitation anomalies are averaged between 15°S and 15°N. The center of each MJO phase is marked on the ordinate axis.

hardly changing at all between Figs. 6a and 6f. Only a small region near California, perhaps, shows weak cancellation, with low height anomalies being slightly more widespread when WP convection is weak. The results taken as a whole again generally support the idea of cancellation between the response to WP and CP convection as highlighted above.

4. Stationary and moving heating

In the previous section, we investigated the sensitivity of the model response to varying strengths of stationary WP and CP convection for the cases of MJO phases 1 and 5 and El Niño and La Niña. In this section, we extend the results of the previous section by investigating the sensitivity of the model response to stationary versus moving heating for all eight MJO phases, as well as testing the sensitivity of the moving heating response to the MJO phase speed.

The day 12–16 model response to the heating associated with stationary convection (the precipitation fields in Fig. 4) is seen in Fig. 7. Although the focus of our study was not to attempt to match the model results with the observations, for reference, we have calculated pattern correlation values between the modeled response over the North Pacific and North America (15°–75°N, 150°E–90°W) for each MJO phase and the observed day 7–14 300-hPa-height DJF composites for each MJO phase over the same region. We find pattern correlation values that range from as low as 0.11 for phase 5 and 0.23 for phase 6 to as high as 0.72 for phase 3 and 0.70 for phase 2. The remaining pattern correlation values fall between 0.40 and 0.50. The observed response to MJO phases 5 and 6 (not shown) shows a height anomaly with a much lower meridional wavenumber than the modeled response, with an Aleutian low extending northward to as far as 75°N, whereas in the model there is a high over Alaska for those phases. This appears to be the major factor in the lower correlation values for those phases. In fact, it appears that the meridional scale is actually too small in the model response for almost all of the MJO phases but that the biggest discrepancy is with MJO phases 5 and 6. This may be in part due to the failure of a dry model to properly capture convective feedbacks in the midlatitude flow. Nevertheless, the model seems to capture the large-scale patterns in the observations quite well, even for transitional phases 4 and 8.

We next focus on the modeled response to individual MJO phases over the North Pacific and western North America. Pattern correlation values over the region from 30° to 75°N and from 180° to 90°W are shown in the bottom-left corner of each panel. For panels that represent MJO phases 1–4, these correspond to the pattern correlations between the given pattern and the MJO phase 1 response to stationary convection for the same model days. Similarly, for panels that represent MJO phases 5–8, these correspond to the pattern correlations between the given pattern and the MJO phase 5 response to stationary convection for the same model days. High positive values thus suggest a similarity in the response to stationary MJO phases 1 or 5. A similar tripole height anomaly pattern is seen for each of MJO phases 1–3 over this region (pattern correlations of 0.83 or higher), with a negative height anomaly over and to the west of Hawaii, another negative height anomaly centered over western Alaska, and a positive height anomaly located about halfway in between. The anomalies are very slightly shifted poleward in phase 3 compared to phase 2 and likewise for phase 2 versus phase 1. The height anomalies are much more amplified in phases 2 and 3 than in phase 1. For phase 4, we see a strong positive height anomaly response centered over the Aleutian Islands, with weaker negative anomalies to the southwest (over Japan) and northeast (northwestern Canada). MJO phases 5–7 show a response with a

Brought to you by NOAA Central Library | Unauthenticated | Downloaded 02/01/21 04:56 PM UTC

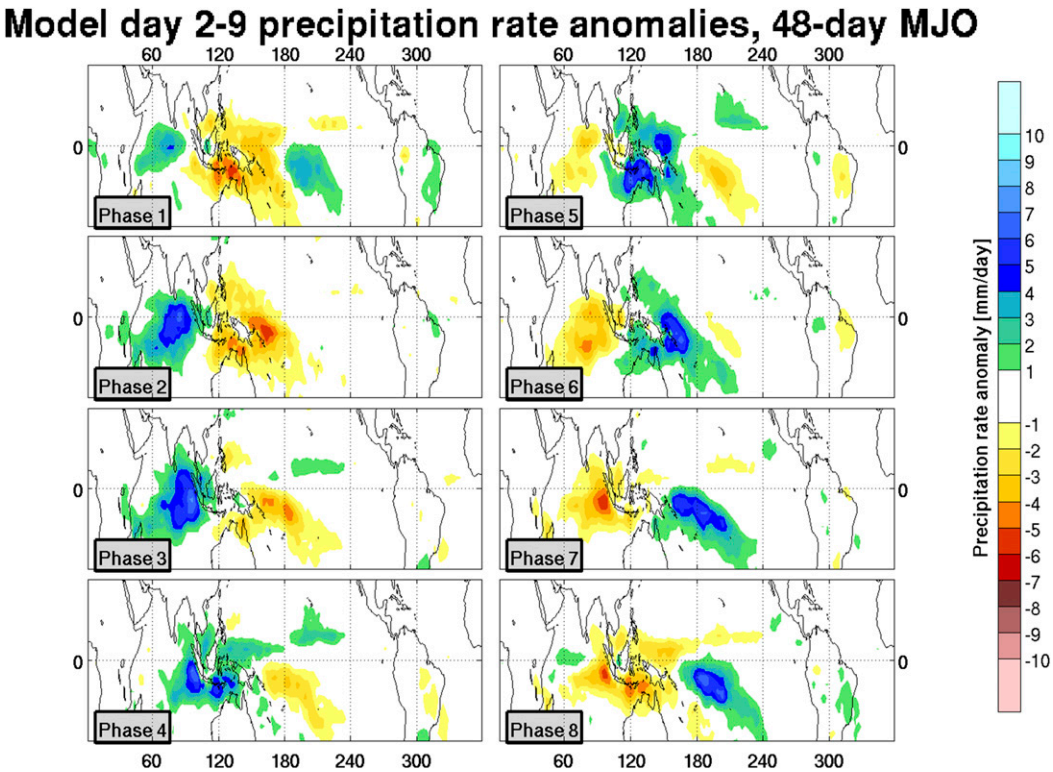

FIG. 9. Mean precipitation anomalies associated with model day 2–9 heating for the moving heating case with a 48-day MJO cycle.

similar spatial structure as for phases 1–3, but with anomalies of opposite sign (pattern correlations of 0.94 or higher). However, the overall amplitude of the tripole is stronger in phase 5 than in phase 1 and weaker in phase 7 than in phase 3. Finally, the response to MJO phase 8 is generally the weakest over the North Pacific and western North America, with only a weak negative anomaly centered over the far northeastern North Pacific. The relatively weak response seen in phase 8 is likely associated with a precipitation signal that is almost equally strong over both the WP and the CP (Fig. 4), consistent with the idea of some cancellation between the responses to convection over those regions. Phases 2–3 and 5–7 show the strongest amplitude response signal, likely associated with the dominance of a single sign in the Pacific precipitation anomalies and, thus, less cancellation in the response. These phases do have strong opposite-signed anomalies located over the Indian Ocean, but based on the results in Goss and Feldstein (2017), which showed that the response to Indian Ocean convection over the North Pacific and North America was weak in both the model and observations, we would not expect these precipitation anomalies to have a large impact over that region. Additionally, the similarities among phases 1–3 (and among phases 5–7) suggest that the Indian Ocean convection, which varies greatly in amplitude over those phases, may not be critical in driving the spatial pattern of the extratropical response, though it may play a role in enhancing the amplitude of the anomalies over the North Pacific. Finally, it might be noticed that the phase 1 and 5 responses are not identical to those seen in Figs. 6k and 7k. It is possible that Indian Ocean convection explains some of this discrepancy, but it is likely that the use of model days 12–16 here rather than days 7–10 explains the largest part of the differences seen.

The day 12–16 model response over Eurasia shows a negative height anomaly stretching from the Caspian Sea to China in phases 1–4, which is centered farther south in phase 1 and gradually transitions northward through phase 4. A strong positive anomaly is seen over South Asia in phases 2–4, with a much weaker positive signal centered over the Indian Ocean in phase 1. Compared with phases 1–4, respectively, opposite-signed anomalies are seen in phases 5–8. This is consistent with the Seo et al. (2016) finding that enhanced convection over the Indian Ocean (seen in the composites for phases 1–4, weakest in phase 1) is associated with an enhanced Hadley cell at those longitudes and, therefore, a stronger subtropical high over South Asia. Likewise, the opposite

Brought to you by NOAA Central Library | Unauthenticated | Downloaded 02/01/21 04:56 PM UTC

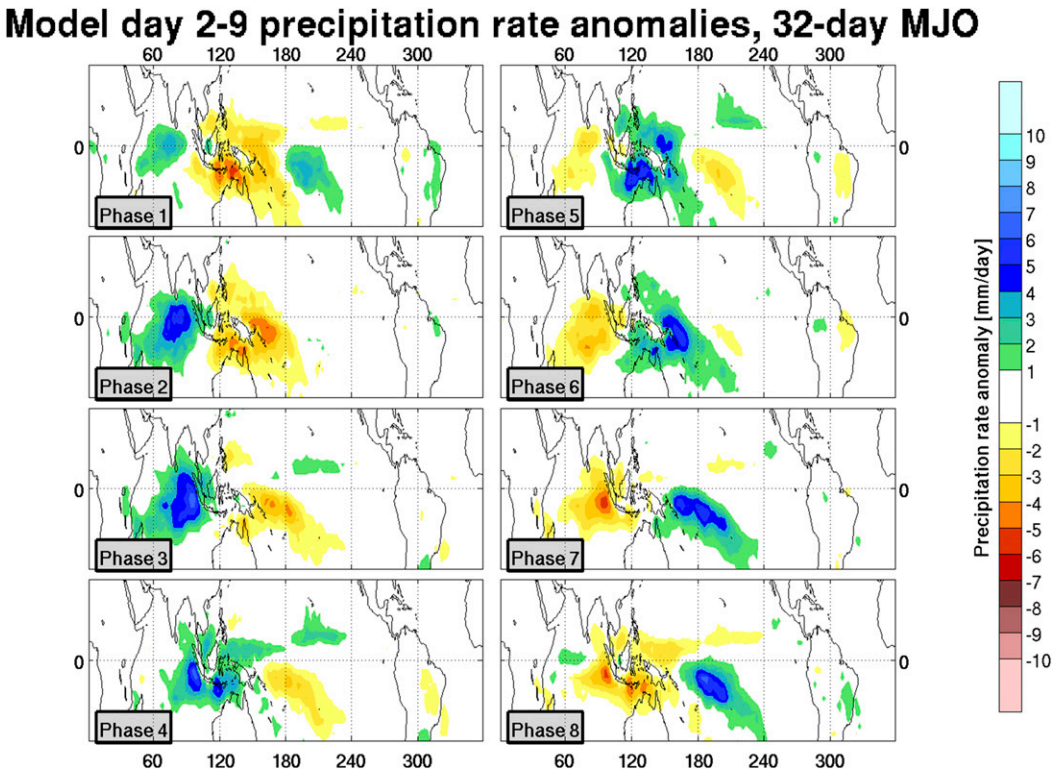

FIG. 10. As in Fig. 9, but for the moving heating case with a 32-day MJO cycle.

occurs with suppressed Indian Ocean convection for MJO phases 5–8.

The 48-day MJO cycle is illustrated in Fig. 8 with a Hovmöller diagram, showing all longitudes, and averaged between latitudes 15°S and 15°N. The ordinate axis is the 48-day cycle, and the center of each MJO phase is marked on that axis. Angle bin 1, corresponding to day 1 of the 48-day cycle, is at the top of the diagram, and angle bin 48 is at the bottom. The 32-day version of the Hovmöller diagram (not shown) is almost identical, and Fig. 8 can be regarded as an approximation for the 32-day cycle if each phase is split into 4 "days" instead of 6. Figures 9 and 10 show the average precipitation composites for days 2–9 of the model run in the 48-day case, and the 32-day case, respectively. As stated above, these model days are chosen because they are centered on the MJO phase being studied (between model days 5 and 6 for the 48-day case and on model day 6 for the 32-day case) and represent model days that are likely to influence the extratropical response at model days 12–16 [Yoo et al. (2012b) showed that the full modeled extratropical response occurs 7–10 days after the MJO heating is fully established]. We see that the precipitation fields in Fig. 9 are almost identical to those in Fig. 4, consistent with the fact that model days 2–9 include only 2 days that are not part of the labeled phase (model day 2 is the last day of the previous phase, and model day 9 is the first day of the following phase). On the other hand, for Fig. 10, model days 2 and 3 are from the previous phase, and model days 8 and 9 are from the following phase. As a result, the precipitation composites for model days 2–9 include more days that are not in the labeled phase. This explains why we see precipitation anomalies in Fig. 10 that are slightly weaker compared to those in Fig. 4.

For each MJO phase, the response to a moving MJO with a 48-day period is seen in Fig. 11. The spatial pattern and amplitude of the response is largely similar to that for the stationary case, with only minor differences. Pattern correlations over the northeastern North Pacific and North America are at or above 0.8 for phases 1–3 and 0.93 or higher for phases 5–7, suggesting a high degree of similarity to the stationary heating cases. However, the amplitude of the response is slightly stronger for MJO phases 1 and 3 in the moving heating case compared to the stationary case. The height anomalies directly associated with the convection over the tropics are seen to be farther east at model days 12–15 in the moving heating case, consistent with a heating source that has progressed eastward in the model. The results in Fig. 11 are intuitive, as the day-2–9 precipitation composites for the 48-day MJO cycle are

Brought to you by NOAA Central Library | Unauthenticated | Downloaded 02/01/21 04:56 PM UTC

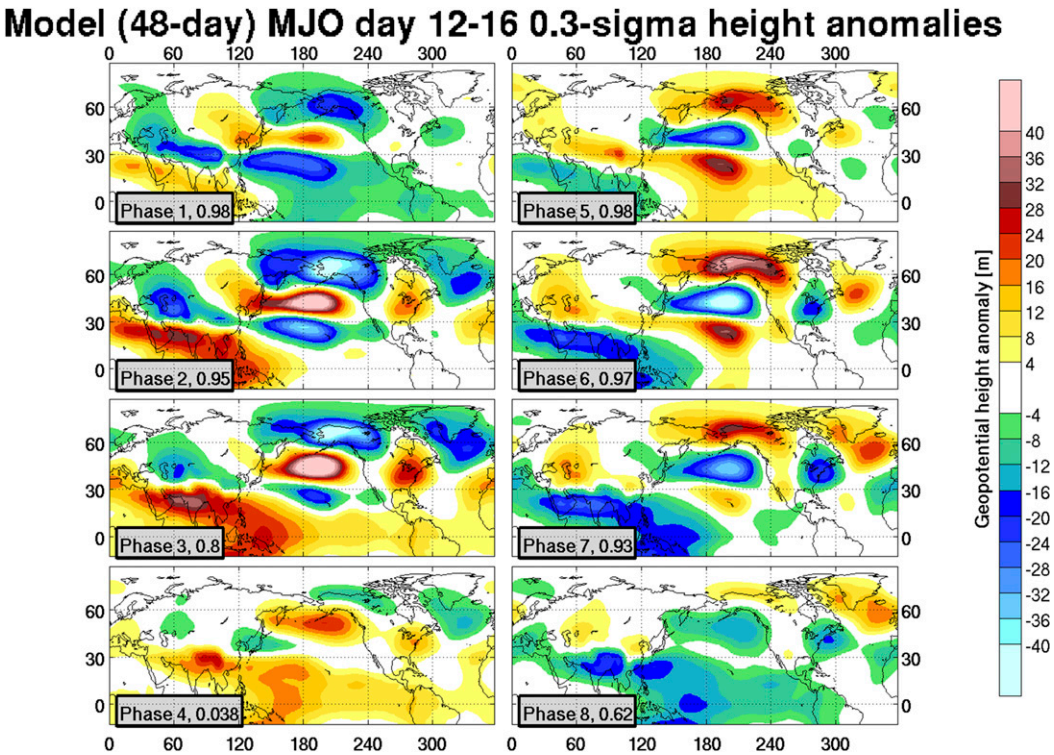

FIG. 11. As in Fig. 7, but for the moving heating case with a 48-day MJO cycle.

very similar to those for the stationary MJO heating (cf. Figs. 3 and 8).

Slightly larger differences are seen when we examine the response to a moving MJO with a 32-day period (Fig. 12). The spatial patterns and amplitudes of the responses are still mostly similar to those in Fig. 7 but are generally slightly weaker, and for MJO phases 1 and 5, the spatial patterns are shifted slightly farther south as well. Pattern correlations are very similar to those in the 48-day-period case, with the biggest differences being for phase 4, a transitional phase (0.04 for the 48-day case, 0.12 for the 32-day case). These differences are very small, and are likely associated with idiosyncratic features of neighboring MJO phases, which have more influence in the faster MJO case. To test the model's sensitivity to unrealistic MJO phase speeds, we also performed an analogous model study using a 16-day period (not shown). The results of this study were broadly similar to those described above, and the differences between the 32-day case and the 16-day case were generally similar to the differences between the 48-day case and the 32-day case, suggesting even further influence from neighboring MJO phases in the 16-day case, as expected. Overall, these results indicate that the model's extratropical response to the MJO exhibits little sensitivity to the propagation speed of the MJO, for all eight MJO phases.

5. Conclusions

In this study, we sought to address the following four key questions: 1) How does the systematic variation of the strength of WP and CP convection anomalies associated with MJO phases 1 and 5, and El Niño and La Niña, affect the extratropical response? 2) What is the modeled extratropical response to stationary heating using realistic precipitation composites for all eight MJO phases? 3) What is the sensitivity of the modeled extratropical response to stationary versus realistic eastward-propagating MJO-like convection for each of the eight phases? 4) What is the sensitivity of the modeled extratropical response to the propagation speed of MJO-like convection for each of the eight phases?

With regard to question 1, we found that the extratropical response over the North Pacific and North America to equatorial convection is strongly sensitive to the relative amplitude of CP and WP convection. Specifically, when the dominant convective signal was for enhanced convection (in either location), we found a positive PNA-like response. The opposite was seen when the dominant convective signal was for suppressed CP or WP convection. Moreover, we found that when the CP and WP convective signals were nearly equal in amplitude but of opposite sign,

Brought to you by NOAA Central Library | Unauthenticated | Downloaded 02/01/21 04:56 PM UTC

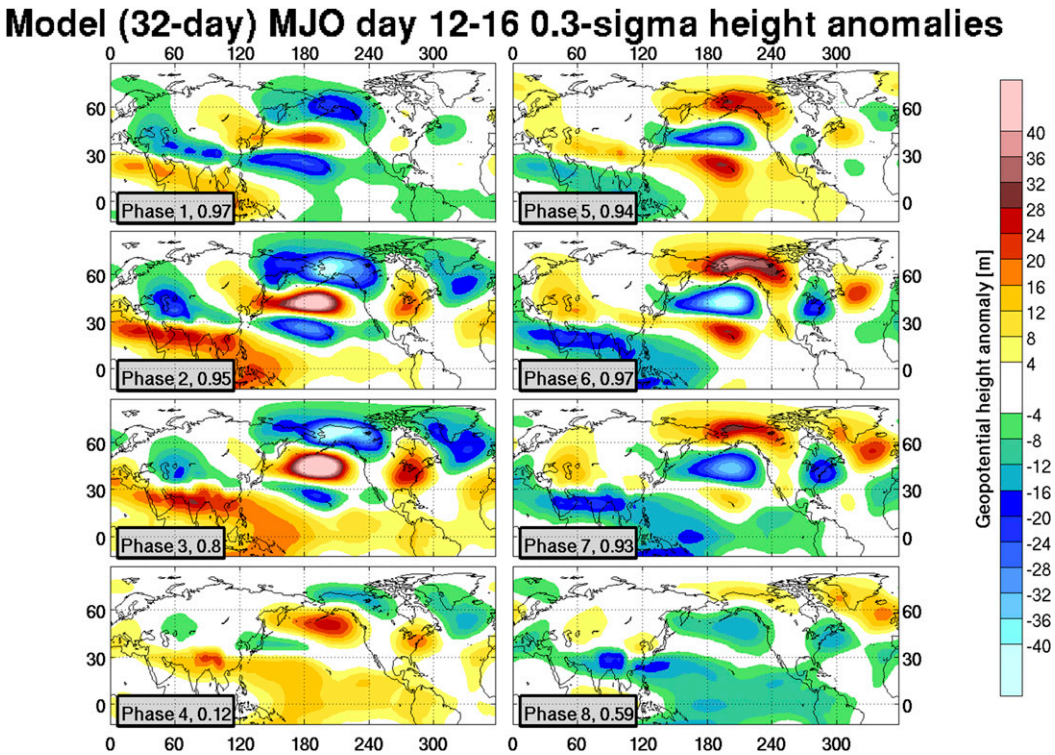

FIG. 12. As in Fig. 7, but for the moving heating case with a 32-day MJO cycle.

although the equatorial precipitation anomalies were relatively strong, a very weak response was seen over the North Pacific and North America, consistent with the idea that there is cancellation associated with the opposite-signed extratropical responses to opposite-signed convective anomalies. These results suggest that, for individual ENSO and MJO cases, since the spatial pattern and amplitude of convection almost certainly varies from case to case, the response is highly sensitive to the exact spatial pattern and relative amplitude of the convection.

For question 2, we found that the extratropical response occurred about 7–10 days after the heating. The response to convection for MJO phases 1–3 over the North Pacific and western North America had similar spatial structures. The response to convection for MJO phases 5–7 also had similar spatial structures, with anomalies of opposite sign compared with those for MJO phases 1–3. Finally, the extratropical response to convection for MJO phases 4 and 8 showed the most unique spatial patterns, being shifted northward from previous phases and having a weaker amplitude. Since phases 4 and 8 featured opposite-signed precipitation anomalies of similar magnitude, these results support the idea of cancellation discussed earlier, leading to the weaker responses seen in those phases. The impact of the Indian Ocean convective anomalies may also explain some of the phase-to-phase differences seen in the model response, especially with respect to the amplitude of the response, but this was not the focus of our study.

For question 3, we found that the extratropical response to propagating MJO heating with a realistic phase speed was almost identical to the stationary case. The minor differences that were seen were likely the result of the effects of neighboring MJO phases. As in the stationary heating case, the extratropical response occurred about 7–10 days after the heating in the given MJO phase. We conclude that, at least for a simple dry dynamical model like the one we used in this study, as long as the spatial structure of the heating is sufficiently accurate, the dynamics that affect the extratropical response are largely captured by a model run with a stationary heating source.

Finally, for question 4, where we examined the extratropical response to a 32-day MJO, our calculations showed slightly bigger differences from the stationary heating case than for the 48-day MJO calculations. However, the differences were still relatively small. As in the previous cases, the response occurred about 7–10 days after the heating in the given MJO phase. Again, these small differences can be explained by the

Brought to you by NOAA Central Library | Unauthenticated | Downloaded 02/01/21 04:56 PM UTC

influence of neighboring MJO phases, which becomes more important for a faster-moving MJO.

Importantly, for questions 3 and 4, our method of defining several MJO phase speeds did not capture the actual observed differences in the horizontal structure of the MJO associated with varying propagation speeds (Yadav and Straus 2017). These differences may arise in part owing to feedback from the extratropical response back onto the MJO's tropical convection. A different MJO phase speed may produce a different interaction between the extratropical response and the MJO convection, which would in turn alter the horizontal structure of the MJO convection. This would then have an impact on the consequent extratropical response. In our study, we aimed to examine how the convective phase speed alone may impact the extratropical response, and therefore, we retained the same spatial structure of the heating between model runs. However, in reality, it is important to note that composites of MJO heating associated with MJO events with varying propagation speeds have a different spatial structure, and therefore it is likely that the extratropical response to MJO events with varying propagation speeds in observations would be substantially different.

Our results imply that special care must be taken when studying the impacts of individual MJO and ENSO cases. Because many such events are characterized by opposite-signed convective anomalies in the WP and CP, the extratropical response is highly sensitive to the exact spatial pattern and amplitude of those convective anomalies. Therefore, each MJO or ENSO event should be examined on a case-by-case basis in order to better understand the observed or forecasted extratropical response. To the extent that these results can be generalized to the real world, this has significant implications for seasonal to subseasonal forecasting, since convection associated with MJO and ENSO events vary on these time scales. For example, if, during an El Niño event, an MJO wave is forecast to propagate through the tropical Pacific in such a way that it strengthens the enhanced CP precipitation anomaly while not significantly impacting the suppressed WP precipitation anomaly, we would expect the response to look like an enhanced version of the El Niño response. However, if the MJO wave weakens the enhanced CP precipitation anomaly while simultaneously strengthening the suppressed WP precipitation anomaly, we may expect a response that does not resemble an El Niño at all, and instead resembles, say, a more standard MJO phase 1 response.

Acknowledgments. This study is supported by National Science Foundation Grants AGS-1401220 and OPP-1723832 and National Oceanic and Atmospheric Administration Grant NA14OAR4310190. We would also like to thank Dr. Paul Roundy and two anonymous reviewers, the European Centre for Medium-Range Weather Forecasts for providing us with the ERA-Interim data that we used for the model climatology, and NOAA's Climate Prediction Center for providing the observed precipitation data.

REFERENCES

Barsugli, J. J., and P. D. Sardeshmukh, 2002: Global atmospheric sensitivity to tropical SST anomalies throughout the Indo-Pacific basin. *J. Climate*, **15**, 3427–3442, https://doi.org/10.1175/1520-0442(2002)015<3427:GASTTS>2.0.CO;2.

Dee, D. P., and Coauthors, 2011: The ERA-Interim reanalysis: Configuration and performance of the data assimilation system. *Quart. J. Roy. Meteor. Soc.*, **137**, 553–597, https://doi.org/10.1002/qj.828.

Goss, M., and S. B. Feldstein, 2015: The impact of the initial flow on the extratropical response to Madden–Julian oscillation convective heating. *Mon. Wea. Rev.*, **143**, 1104–1121, https://doi.org/10.1175/MWR-D-14-00141.1.

——, and ——, 2017: Why do similar patterns of tropical convection yield extratropical circulation anomalies of opposite sign? *J. Atmos. Sci.*, **74**, 487–511, https://doi.org/10.1175/JAS-D-16-0067.1.

Held, I. M., and M. J. Suarez, 1994: A proposal for the intercomparison of the dynamical cores of atmospheric general circulation models. *Bull. Amer. Meteor. Soc.*, **75**, 1825–1830, https://doi.org/10.1175/1520-0477(1994)075<1825:APFTIO>2.0.CO;2.

Hoskins, B. J., and D. J. Karoly, 1981: The steady linear response of a spherical atmosphere to thermal and orographic forcing. *J. Atmos. Sci.*, **38**, 1179–1196, https://doi.org/10.1175/1520-0469(1981)038<1179:TSLROA>2.0.CO;2.

Johnson, N. C., D. C. Collins, S. B. Feldstein, M. L. L'Heureux, and E. E. Riddle, 2014: Skillful wintertime North American temperature forecasts out to 4 weeks based on the state of ENSO and the MJO. *Wea. Forecasting*, **29**, 23–38, https://doi.org/10.1175/WAF-D-13-00102.1.

Madden, R. A., and P. R. Julian, 1971: Detection of a 40–50 day oscillation in the zonal wind in the tropical Pacific. *J. Atmos. Sci.*, **28**, 702–708, https://doi.org/10.1175/1520-0469(1971)028<0702:DOADOI>2.0.CO;2.

——, and ——, 1972: Description of global-scale circulation cells in the tropics with a 40–50 day period. *J. Atmos. Sci.*, **29**, 1109–1123, https://doi.org/10.1175/1520-0469(1972)029<1109:DOGSCC>2.0.CO;2.

Rasmusson, E. M., and T. H. Carpenter, 1982: Variations in tropical sea surface temperature and surface wind fields associated with the Southern Oscillation/El Niño. *Mon. Wea. Rev.*, **110**, 354–384, https://doi.org/10.1175/1520-0493(1982)110<0354:VITSST>2.0.CO;2.

——, and J. M. Wallace, 1983: Meteorological aspects of the El Niño/Southern Oscillation. *Science*, **222**, 1195–1202, https://doi.org/10.1126/science.222.4629.1195.

Seo, K.-H., and S.-W. Son, 2012: The global atmospheric circulation response to tropical diabatic heating associated with the Madden–Julian oscillation during northern winter. *J. Atmos. Sci.*, **69**, 79–96, https://doi.org/10.1175/2011JAS3686.1.

——, H.-J. Lee, and D. M. Frierson, 2016: Unraveling the teleconnection mechanisms that induce wintertime temperature anomalies over the Northern Hemisphere continents in response to the MJO. *J. Atmos. Sci.*, **73**, 3557–3571, https://doi.org/10.1175/JAS-D-16-0036.1.

Brought to you by NOAA Central Library | Unauthenticated | Downloaded 02/01/21 04:56 PM UTC

Ting, M., and P. D. Sardeshmukh, 1993: Factors determining the extratropical response to equatorial diabatic heating anomalies. *J. Atmos. Sci.*, **50**, 907–918, https://doi.org/10.1175/1520-0469(1993)050<0907:FDTERT>2.0.CO;2.

Wheeler, M. C., and H. H. Hendon, 2004: An all-season real-time multivariate MJO index: Development of an index for monitoring and prediction. *Mon. Wea. Rev.*, **132**, 1917–1932, https://doi.org/10.1175/1520-0493(2004)132<1917:AARMMI>2.0.CO;2.

Xie, P., and P. A. Arkin, 1997: Global precipitation: A 17-year monthly analysis based on gauge observations, satellite estimates, and numerical model outputs. *Bull. Amer. Meteor. Soc.*, **78**, 2539–2558, https://doi.org/10.1175/1520-0477(1997)078<2539:GPAYMA>2.0.CO;2.

Yadav, P., and D. M. Straus, 2017: Circulation response to fast and slow MJO episodes. *Mon. Wea. Rev.*, **145**, 1577–1596, https://doi.org/10.1175/MWR-D-16-0352.1.

Yoo, C., S. Lee, and S. B. Feldstein, 2012a: Mechanisms of extratropical surface air temperature change in response to the Madden–Julian oscillation. *J. Climate*, **25**, 5777–5790, https://doi.org/10.1175/JCLI-D-11-00566.1.

——, ——, and ——, 2012b: Arctic response to an MJO-like tropical heating in an idealized GCM. *J. Atmos. Sci.*, **69**, 2379–2393, https://doi.org/10.1175/JAS-D-11-0261.1.

Zhang, C., J. Gottschalck, E. D. Maloney, M. W. Moncrieff, F. Vitart, D. E. Waliser, B. Wang, and M. C. Wheeler, 2013: Cracking the MJO nut. *Geophys. Res. Lett.*, **40**, 1223–1230, https://doi.org/10.1002/grl.50244.

Brought to you by NOAA Central Library | Unauthenticated | Downloaded 02/01/21 04:56 PM UTC